https://doi.org/10.1007/s41230-019-9071-0

Solidification sequence and as-cast microstructure of a model Pb-Bi-Sn alloy with quasi-peritectic reaction

Gang Liu[1], Qian Yang[1], Cao Wang[1], Zhu-huan Yu [2, 3], *Guo-jun Zhang[1]

1. School of Materials Science and Engineering, Xi'an University of Technology, Xi'an 710048, China

2. School of Materials Science and Engineering, Xi'an University of Science and Technology, Xi'an710054, China

3. State Key Laboratory of Solidification Processing, Northwestern Polytechnical University, Xi'an 710072, China

Abstract: The $Pb_{39}Bi_{25}Sn_{36}$ alloy was directionally solidified at varied withdrawal rates followed by quenching. From metallographic observation, composition analysis and differential scanning calorimetry (DSC) analysis, the solidification sequence of $Pb_{39}Bi_{25}Sn_{36}$ alloy was characterized. The Sn-dendrite is observed as the primary phase during solidification, followed by the β(Pb_7 Bi_3)/Sn divorced eutectic. At lower temperatures, the β(Pb_7Bi_3)/Sn binary eutectic is formed in the interdendritic region. However, the quasi-peritectic reaction [L+α-Pb→β(Pb_7 Bi_3)+Sn] does not occur as the prediction based on ternary phase diagram analysis, which can be attributed to the unequilibrium solidfication condition. Moreover, the as-cast microstructure is significantly refined with the increasing withdrawal rates. The quenched sample only exhibits the lamellar structure of Sn, β(Pb_7Bi_3) and Bi phases. The results can provide instructions to optimize the as-cast microstructure of ternary alloys with quasi-peritectic reaction.

Key words: quasi-peritectic alloy; directional solidification; solidification sequence

CLC numbers: TG146.1+2 **Document code:** A **Article ID:** 1672-6421(2019)06-399-07

In the past few decades, the solidification behavior of binary alloys with dendritic, eutectic or peritectic reactions has been widely investigated. However, the alloys for industrial application are multicomponent alloys. The quasi-peritectic reaction, which was defined as: L+α→β+γ, where L indicates the liquid phase, and α, β, and γ indicate the solid phases, are usually observed during solidification of multicomponent alloys. For example, G. Sha et al. [1] investigated the as-cast microstructure of Al-Si-Fe alloys, and found two quasi-peritectic reactions: L+$Al_{13}Fe_4$→α-AlFeSi+α-Al and L+α-AlFeSi→β-AlFeSi+α-Al. Additionally, the quasi-peritectic reaction was also observed during solidification of solder alloys, such as Cu-Ni-Sn [2], Pb-Bi-Sn [3] and Cu-Sn-Zn [4]. Recently, refractory alloys, such as Ta-Al-Fe[5, 6] and Nb-Al-Co [7], which were treated as the potential high-temperature structural materials, also exhibit quasi-peritectic reaction. The solidification behavior of ternary alloys are much more complicated than the counterpart of binary alloys. Particularly, the solidification parameters, such as thermal gradient and cooling rate, have strong effects on the morphology, size, and distribution of strengthening phase of the multiphase alloys. To improve the mechanical properties of ternary alloys with a quasi-peritectic reaction, it is necessary to clarify the solidification behavior.

In this investigation, the Pb-Bi-Sn alloy was selected as the model alloy, because it contains the eutectic (L→α-Pb+Sn; L→β(Pb_7Bi_3)+Sn) and quasi-peritectic reactions (L+α-Pb→β-Pb_7Bi_3+Sn). Due to the varied solidification parameters, it is difficult to characterize the solidification sequence of ternary alloys with conventional casting or arc-melting techniques. Fortunately, the directional solidification technique provides a convenient way to characterize the solidification patterns by observing the quenched microstructure in the mushy zone. Consequently, the Pb-Bi-Sn alloy was directionally solidified followed by quenching to investigate the microstructural evolution. Furthermore, the influence of withdrawal rate on solidification sequence of the Pb-Bi-Sn alloy was discussed.

1 Materials and methods

The $Pb_{39}Bi_{25}Sn_{36}$ (wt.%) ingots, weighing ~400 g, were prepared by the resistance heating furnace with graphite crucibles. To guarantee homogenization, the melt was stirred during the melting process. As-cast Φ7 mm×110 mm rods were cut from the ingots by

***Guo-jun Zhang**

Male, born in 1974, Professor. His research interests mainly focus on the microstructure control and mechanical properties of nonferrous metals.

E-mail: zhangguojun@xaut.edu.cn

Received: 2019-05-24; Accepted: 2019-09-10

wire electro-discharged machine and placed in a high purity alumina crucible for directional solidification. The Bridgman furnace was heated to 450 °C to melt the sample, and then it was held for 20 min to homogenize the melt. Then, the sample was directionally solidified at different withdrawal rates of 10, 50, and 100 μm·s^{-1}, respectively, followed by quenching into the Ga-In-Sn liquid metal. The thermal gradient close to the solid/liquid interface was calculated to be approximately 110 K·cm^{-1}. Approximately 50 mg of the as-cast sample was used for differential scanning calorimetry (DSC, STA449F3) analysis. Samples were heated to 400 °C at the heating rate of 10 °C·min^{-1} in a flowing stream of Ar. The phases were characterized by X-Ray diffractometer (SHIMADZU XRD-7000). The directionally solidified microstructure was analyzed by an optical microscope (OLYMPUS GX71/50) and a scanning electron microscope (SEM, JSM-6700F) with energy dispersive spectrometry (EDS).

2 Results

2.1 Solidification sequence analyzed by ternary phase diagram and thermodynamic calculation

The composition of $Pb_{39}Bi_{25}Sn_{36}$ (wt.%) is indicated on the liquid projection of Pb-Bi-Sn ternary alloy [8-9] (Fig. 1). According to the equilibrium liquid projection, $Pb_{39}Bi_{25}Sn_{36}$ (wt.%) alloy undergoes four reactions, as follows:

$$T_L \approx 148\ °C,\ L \rightarrow Sn \quad (1)$$

$$T_{E1} = 137.4\text{–}148\ °C,\ L \rightarrow (\alpha\text{-Pb/Sn})_{eutectic} \quad (2)$$

$$T_{U1} = 137.4\ °C\ [9],\ L + \alpha\text{-Pb} \rightarrow \beta(Pb_7Bi_3) + Sn \quad (3)$$

$$T_{E2} = 100\text{–}137.4\ °C,\ L \rightarrow (\beta(Pb_7Bi_3)/Sn)_{eutectic} \quad (4)$$

where T_L, T_{E1}, T_{U1} and T_{E2} correspond to the liquidus, α-Pb/Sn eutectic, quasi-peritectic, and $\beta(Pb_7Bi_3)$/Sn eutectic temperatures, respectively. The Sn firstly solidified from liquid as the primary phase. Subsequently, the composition of liquid varied along the monovariant line of the α-Pb/Sn eutectic valley. Then, the quasi-peritectic microstructure is formed at T_{U1}. Finally, $\beta(Pb_7Bi_3)$/Sn eutectic solidified from the remaining liquid at the lower temperature.

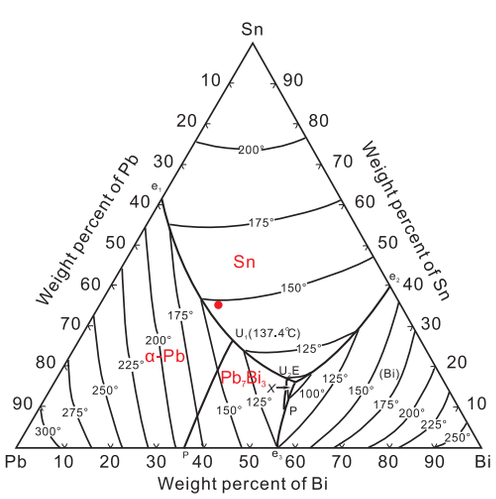

Fig. 1: Liquid projection of Pb-Bi-Sn ternary alloy[9]

To further clarify the solidification sequence of $Pb_{39}Bi_{25}Sn_{36}$ alloy, the equilibrium mole fraction of constituent phases as a function of temperature was calculated by the thermodynamic software JMatPro. As shown in Fig. 2, the Sn firstly solidified from the melt as the primary phase, followed by the $\beta(Pb_7Bi_3)$ and Sn dual-phases structure. Due to the solid precipitation at lower temperatures, the final microstructure consists of the $\beta(Pb_7Bi_3)$, Sn and Bi phases. The α-Pb phase, as predicted by the ternary phase diagram, does not exist by thermodynamic calculation.

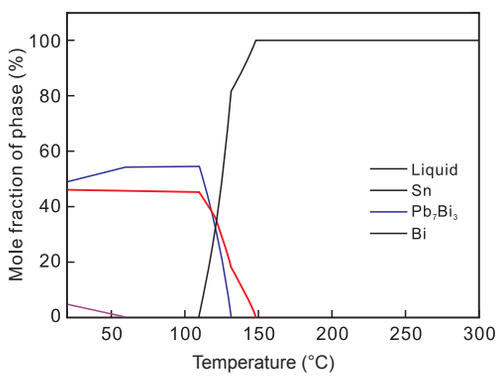

Fig. 2: Equilibrium mole fraction of various phases as a function of temperature for $Pb_{39}Bi_{25}Sn_{36}$ alloy

To confirm the phase constitution, the directionally solidified and quenched samples were characterized by the X-ray diffraction (XRD) analysis (Fig. 3). Individual phases were identified with the JCPDS databases (major phases, Sn:04–0673 and Pb_7Bi_3:39–1087; minor phases Bi:85–1329) and marked with different symbols. Figure 3 shows the overview of the measured XRD patterns of the samples with varied withdrawal rates. In all cases, the XRD peaks can be indexed as $\beta(Pb_7Bi_3)$, Sn and Bi phases, which are consistent with the results of thermodynamic calculation.

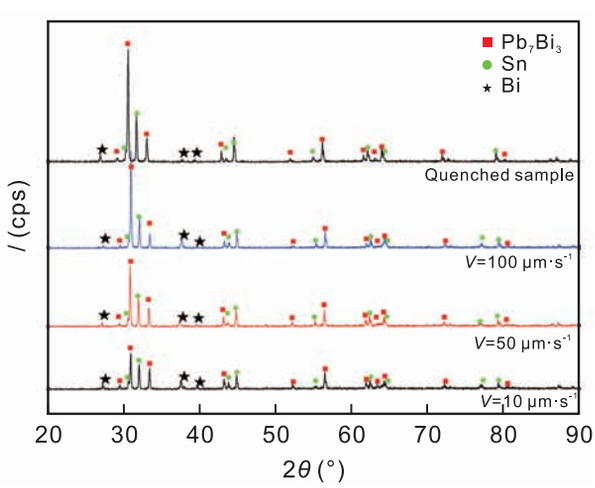

Fig. 3: X-ray diffraction data for directionally solidified and quenched $Pb_{39}Bi_{25}Sn_{36}$ samples

2.2 Formation and microstructure evolution of mushy zone

Figure 4 shows the optical and backscattered electron images of the sample solidified at the withdrawal rate of 10 μm·s^{-1}.

(It should be noted that the optical and SEM images exhibit different contrast for the same phase). Due to the upward thermal gradient, the heat flux is antiparallel to the growth direction of the solid/liquid interface. From top to bottom, the mushy zone can be apparently divided into three parts. The upper section shows the quenched solid/liquid interface [Fig. 4(b)]. As expected, the primary phase with dendritic morphology is Sn (Table 1). The middle part exhibits a mushy zone with primary Sn-dendrite surrounded by $\beta(Pb_7Bi_3)$ phase [Fig. 4(c)]. Subsequently, the remaining liquid is quenched. The bottom section exhibits the similar dendritic structure, but surrounded with the higher amount of $\beta(Pb_7Bi_3)$ phase. In contrast to the middle section, the additional $\beta(Pb_7Bi_3)$/Sn eutectic [Fig. 4(d)] is found in the interdendritic region. Figure 5 shows the corresponding enlarged region of quenched liquid [marked by blue rectangle in Fig. 4(d)]. The quenched liquid consists of Sn, $\beta(Pb_7Bi_3)$ and Bi phases. Due to the similar atomic numbers of Pb (82) and Bi (83), the backscattered electron image (BEI) only shows the inconspicuous contrast between $\beta(Pb_7Bi_3)$ and Bi phases. Moreover, the chemical compositions of the above mentioned phases are shown in Table 1.

It is convenient to study the solidification sequence in the mushy zone with the directional solidification technique. Based on the above microstructural observation, the solidification sequence of $Pb_{39}Bi_{25}Sn_{36}$ (wt.%) alloy can be described as follows:

$$L \rightarrow Sn_{dendrite} + L_1$$
$$\rightarrow Sn_{dendrite} + [\beta(Pb_7Bi_3)/Sn]_{divorced\text{-}eutectic} + L_2$$
$$\rightarrow Sn_{dendrite} + [(\beta(Pb_7Bi_3)/Sn]_{divorced\text{-}eutectic} + [\beta(Pb_7Bi_3)/Sn)]_{eutectic} + L_3$$

where L_1, L_2 and L_3 are the remaining liquid in the mushy zone. During the solidification process, the Sn-dendrite firstly solidified as the primary phase. Consequently, the $\beta(Pb_7Bi_3)$/Sn solidified as the divorced eutectic along the boundary of primary Sn-dendrite. When the composition of L_2 meets the monovariant line

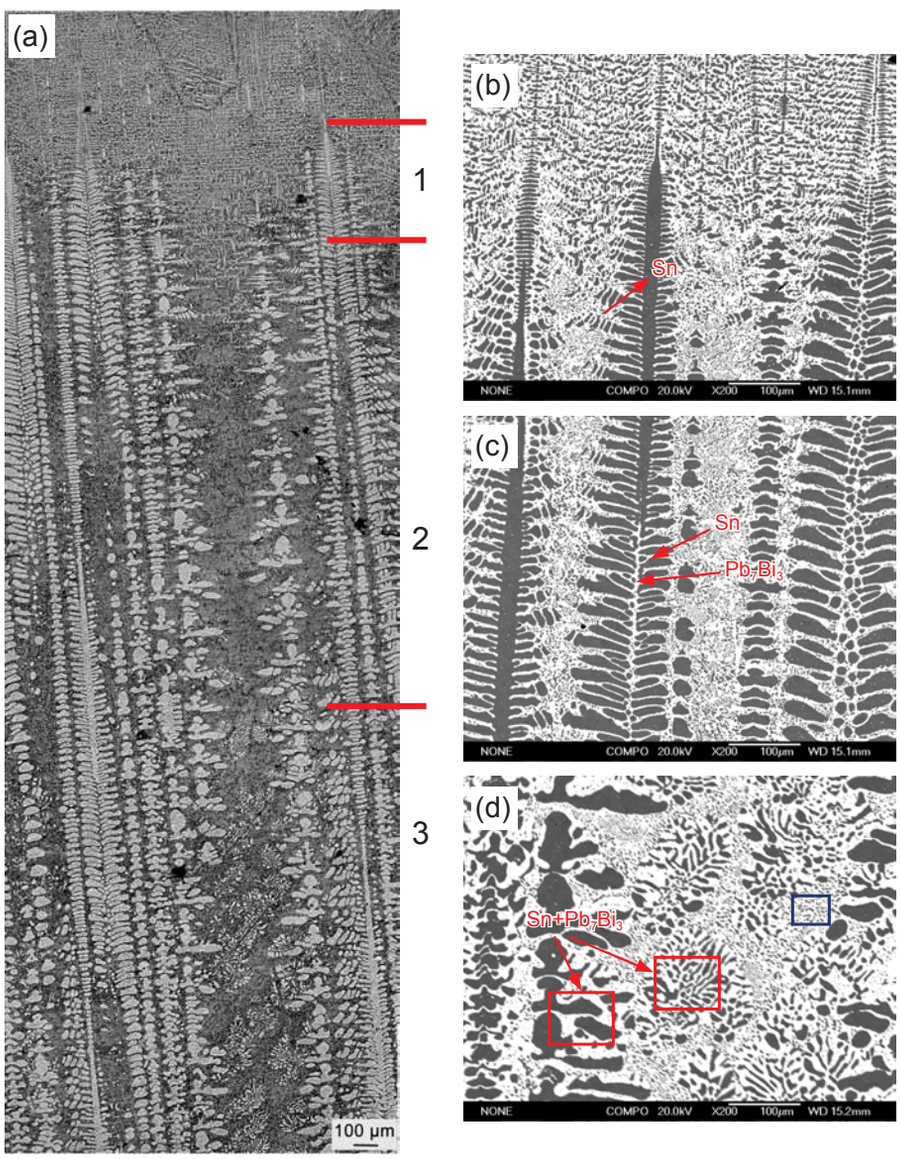

Fig. 4: Optical and backscattered electron SEM images of the directionally solidified $Pb_{39}Bi_{25}Sn_{36}$ alloy: (a) Optical image of mushy zone; (b) SEM image of the upper section of mushy zone (Zone 1); (c) SEM image of the middle section of mushy zone (Zone 2); (d) SEM image of the bottom section of mushy zone (Zone 3)

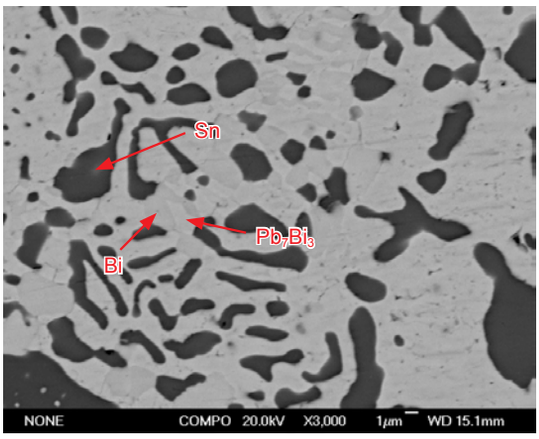

Fig. 5: Backscattered electron SEM images of quenched liquid [marked by the blue rectangle in Fig. 4(d)]

Table 1: Average composition (wt.%) of phases at different locations shown in Fig.4

Test zone	Phase	Pb	Bi	Sn
Upper section	Sn	1.38	4.86	93.76
Middle section	Sn	1.24	4.39	94.37
Bottom section	β(Pb_7Bi_3)	67.68	29.90	2.42
	Sn	1.26	5.24	93.50
Quenched liquid	β(Pb_7Bi_3)	67.97	29.47	2.56
	Sn	5.99	7.14	86.86
	β(Pb_7Bi_3)	64.18	29.69	6.13
	Bi	8.02	84.51	7.47

of [β(Pb_7Bi_3)/Sn)]$_{eutectic}$ (line U_1U_2 shown in Fig. 1), the β(Pb_7Bi_3)/Sn eutectic solidified in the interdendritic region. Then, according to Pb-Bi-Sn ternary phase diagram (Fig. 1), the remaining liquid (L_3) will undergo the quasi-peritectic reaction at Point U_2 [L+β(Pb_7Bi_3)→*X*+Sn] and ternary eutectic reaction (L→*X*+Sn+Bi) at Point E. The *X* phase has been proved to be a Pb-Bi-Sn metastable phase [9], which will transform to β(Pb_7Bi_3)+Sn+Bi by eutectoid reaction at 78 °C. Due to the limited remaining liquid at the final stage of solidification, only a small amount of Bi can be detected in the as-cast microstructure (Fig. 5).

2.3 Characteristic phase transformation temperature analyzed by DSC

To further clarify the solidification sequence, DSC was used to detect the characteristic phase transformation temperature of $Pb_{39}Bi_{25}Sn_{36}$ alloy at the heating rate of 10 K·min^{-1}. As shown in Fig. 6, five endothermic peaks can be clearly observed in the temperature range of 75–175 °C. Referring to the ternary phase diagram (Fig. 1) and microstructural observation (Section 2.2), the first endothermic peak at 96.0 °C is related to the ternary eutectic reaction L→Sn+*X*+Bi. The second endothermic peak at 99.7 °C is related to the quasi-peritectic reaction at Point U_2 [L+β(Pb_7Bi_3)→Sn+*X*]. The third endothermic peak at 124.6 °C is associated with the monovariant line of β(Pb_7Bi_3)/Sn eutectic valley. Based on microstructural observation, the fourth

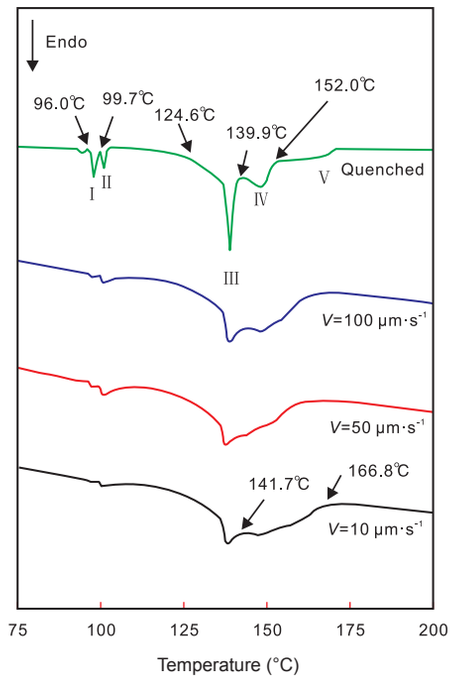

Fig. 6: DSC thermal analysis of $Pb_{39}Bi_{25}Sn_{36}$ alloy

endothermic peak at 139.9 °C is associated with the melt of divorced eutectic β(Pb_7Bi_3)/Sn. Finally, the endothermic peak at 152.0 °C is related to the melt of primary Sn phase. Due to the higher fraction of primary Sn-dendrite (shown in Section 2.4), the endothermic peaks Ⅳ and Ⅴ are much more overlapped for directionally solidified samples than the counterpart of the quenched sample.

Moreover, the thermal gradient can be estimated by analyzing the DSC results (Fig. 6) and quenched microstructure of the directionally solidified sample at the withdrawal rate of 10 μm·s^{-1} (Fig. 4). As shown in the DSC curve, the liquidus and the temperature of β(Pb_7Bi_3)/Sn divorced eutectic is 166.8 °C and 141.7 °C, respectively. Consequently, the freezing range from the primary Sn-dendrite to [β(Pb_7Bi_3)/Sn] divorced eutectic is 25.1 °C. The corresponding distance from the dendrite tip (Zone 1 in Fig. 4) to the divorced eutectic of β(Pb_7Bi_3)/Sn (Zone 2 in Fig. 4) is 2.22 mm. Therefore, the thermal gradient of approximately 110 K·cm^{-1} can be calculated by the ratios of freezing range to the corresponding distance.

2.4 Dependence of as-cast microstructure on withdrawal rate

The primary dendrite arm spacing (λ_1) and secondary dendrite arm spacing (λ_2) are the characteristic lengths of as-cast microstructure, which have significant influence on microsegregation and solidification patterns. Many models have been used to characterize the relationship among λ_1, λ_2, and the solidification parameters, such as withdrawal rate (V), and thermal gradient (G), as proposed by the Hunt model [10]:

$$\lambda_1=2.83(k\Delta T_0\Gamma D)^{\frac{1}{4}}G^{-\frac{1}{2}}V^{-\frac{1}{4}} \quad (1)$$

where k is the equilibrium partition coefficient, ΔT_0 is the freezing range, Γ is the Gibbs-Thomson coefficient, D is the diffusion coefficient in liquid, G is the thermal gradient and V is

the withdrawal rate. Additionally, the Flemings model [11]gave the λ_2 as:

$$\lambda 2 = 5.5\left[\frac{\Gamma D}{m(1-k)(C0-Ce)} In\left(\frac{Ce}{C0}tf\right)\right]^{\frac{1}{3}} \quad (2)$$

$$t_f=\Delta T_0/GV \quad (3)$$

where m is the slope of liquidus, C_0 and Ce are the nominal and eutectic composition of alloy, t_f is the local solidification time. Base on the Equations (1) and (2), the increased V leads to the higher cooling rate, thus resulting in the refined dendritic microstructure.

Figure 7 exhibits the longitudinal and cross-sectional microstructures of the directionally solidified $Pb_{39}Bi_{25}Sn_{36}$ at different withdrawal rates. The Sn-dendrite (black) surrounded by the β(Pb_7Bi_3) phase (grey) can be clearly observed [Fig. 7(b)]. As expected, the dendrite structure is significantly refined at the higher withdrawal rates. Figure 8 shows the variations of λ_1, λ_2, and area fraction of Sn-dendrite with the withdrawal rate. As shown in Fig. 8, the values of λ_1 and λ_2 reduced from 157.2 and 35.6 μm to 81.8 and 9.0 μm, respectively, as the withdrawal rate increased from 10 to 100 μm·s^{-1}. Meanwhile, the primary Sn dendrite is suppressed at the higher withdrawal rate. Particularly, the quenched sample [Figs. 7(g-h)] only exhibits

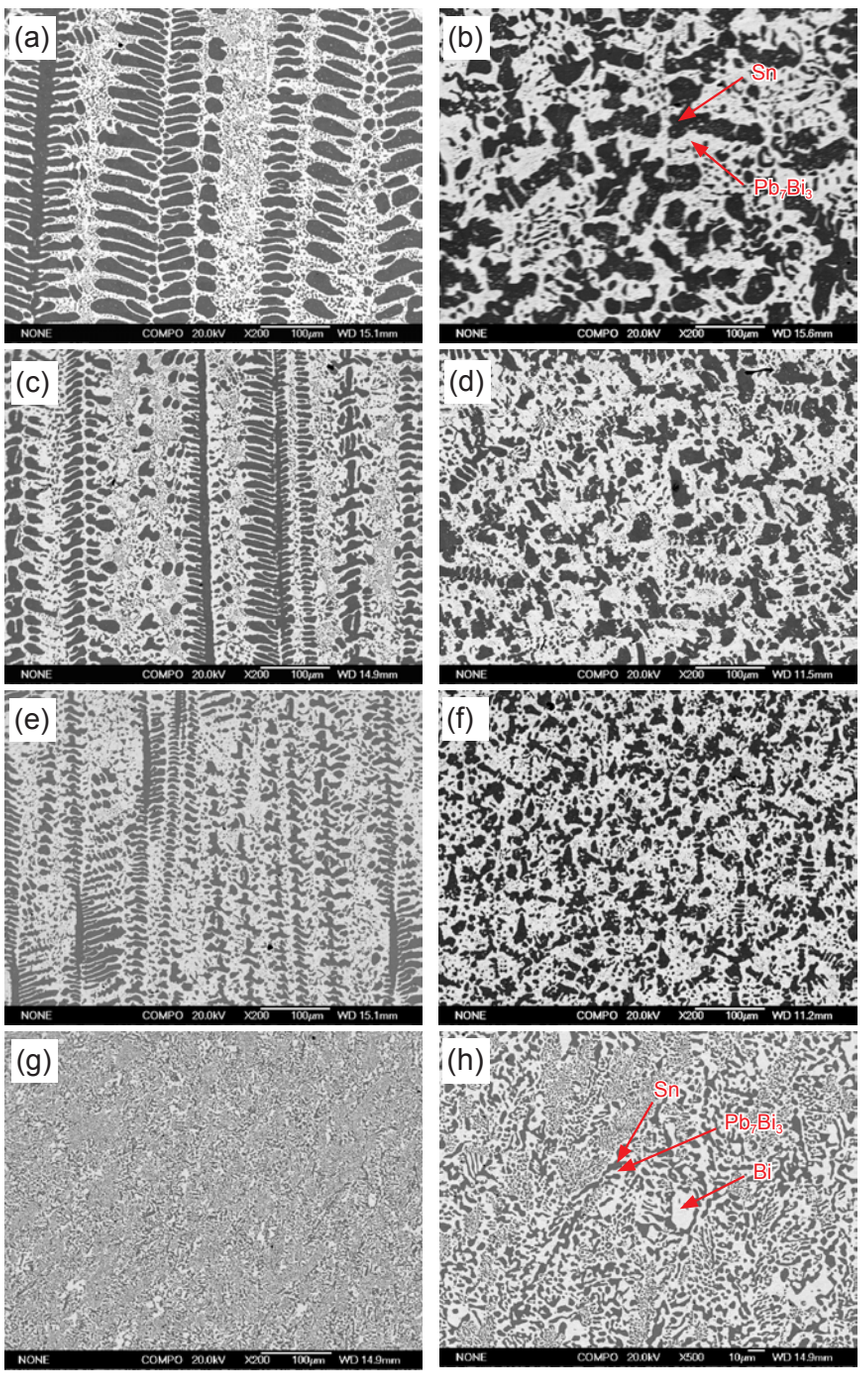

Fig. 7: Microstructures of directionally solidified $Pb_{39}Bi_{25}Sn_{36}$ alloy at different withdrawal rates (V): (a, c, e) Longitudinal microstructures, V=10, 50 and 100 μm·s^{-1}, respectively; (b, d, f) Cross-sectional microstructure, V=10, 50 and 100 μm·s^{-1}, respectively; (g, h) SEM images of quenched sample at low and high magnifications, respectively

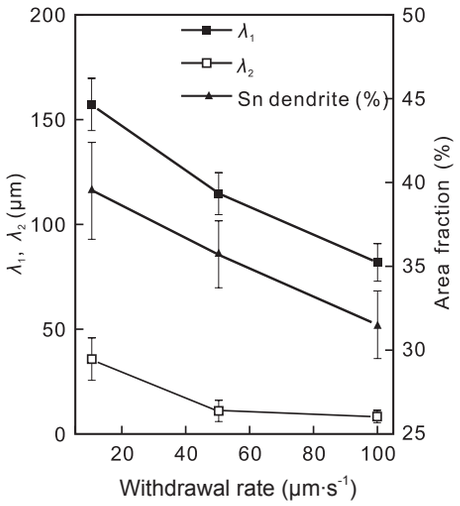

Fig. 8: Variation of primary dendrite arm spacing (λ_1), secondary dendrite arm spacing (λ_2) and area fraction of Sn-dendrite at different withdrawal rates

the lamellar microstructures, which consists of Sn, β(Pb_7Bi_3) and Bi phases.

3 Discussion

Figure 9 shows the quasi-peritectic reaction of Pb-Bi-Sn alloy. Four phases are involved in the quasi-peritectic reaction: L+α-Pb→β(Pb_7Bi_3)+Sn. There are two monovariant three-phase equilibria [L-Sn-α-Pb, L-α-Pb-β(Pb_7Bi_3)] above the quasi-peritectic isotherm [Fig. 9(a)], while two three-phase equilibria [L-Sn-β(Pb_7Bi_3), α-Pb-Sn-β(Pb_7Bi_3)] below the quasi-peritectic isotherm [Fig. 9(b)]. For this study, $Pb_{39}Bi_{25}Sn_{36}$ locates near the monovariant line of the Sn/α-Pb eutectic valley. On the equilibrium condition, Sn firstly solidified from the melt, followed by Sn/α-Pb eutectic. Then, β(Pb_7Bi_3)/Sn quasi-peritectic is formed at the invariant temperature. After the quasi-peritectic reaction, the remaining liquid will solidify along the monovariant line β(Pb_7Bi_3)/Sn eutectic.

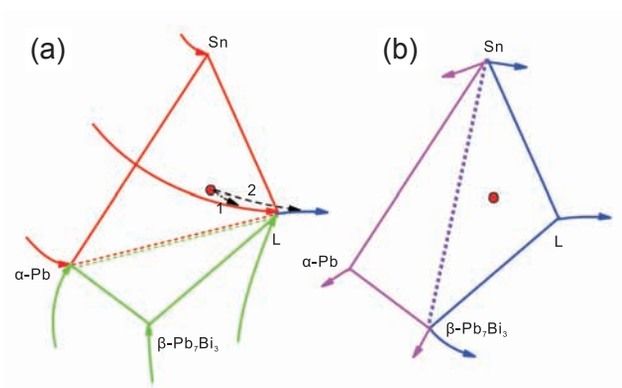

Fig. 9: Schematic of quasi-peritectic reaction [L+α-Pb→β(Pb_7Bi_3)+Sn]: (a) Three-phase reaction before quasi-peritectic reaction; (b) Three-phase reaction after quasi-peritectic reaction

However, the above solidification sequence is based on the equilibrium thermodynamical analysis. Similar with the peritectic reaction of binary alloy [12, 13], the quasi-peritectic reaction must occur under the undercooling condition to achieve the driving force. Meanwhile, the third phase formed by the quasi-peritectic reaction will adhere to the existing phase, thus inhibiting the subsequent quasi-peritectic reaction. The quasi-peritectic transformation depends on the diffusion in liquid and dissolution of α-Pb. Since the solidification process in this study deviates from the equilibrium condition, it will lead to the residual α-Pb in as-cast microstructure. However, even for the quenched sample, the α-Pb phase has not been detected by XRD and microstructural analysis. Therefore, it can be concluded that the quasi-peritectic reaction [L+α-Pb→β(Pb_7Bi_3)+Sn] does not occur as expected.

Due to the added degree of freedom, the solidification sequence of ternary alloys is much more complicated than the counterpart of binary alloys. The phase rule at constant pressure is described as:

$$F=C-P+1$$

where F is the number of degrees of freedom, C is the number of components and P is the number of phases. During solidification of the primary phase, two-phase equilibria is reached. The phase rule of ternary alloy is F=3-2+1=2. Therefore, the temperature and composition can be changed independently to keep two-phase equilibria. Consequently, the route traversed by liquid composition on the liquidus surface has different choices, which is closely related with the alloy composition and solidification parameters, such as the cooling rate, back-diffusion in the solid, partition coefficient, and so on. Not only the evolution of primary phase, but also the following type of three-phase equilibria depended on the intersecting point of liquidus and the monovariant line. As shown in Fig. 9, two different routes are marked on the liquidus surface projection. For Path 1, the intersecting point is located on the monovariant line of L-Sn-α-Pb equilibria, indicating the occurrence of α-Pb/Sn eutectic after the solidification of primary Sn phase. In contrast, Path 2 intersects with the monovariant line of L-Sn-β(Pb_7Bi_3), thus indicating the occurrence of β(Pb_7Bi_3)/Sn eutectic after the solidification of primary Sn phase. The occurrence of invariant quasi-peritectic reaction depends on the solidification path. The similar phenomenon was also observed in other ternary alloy systems, such as Ta-Al-Fe [5], Pb-Sn-Sb [14] and Nb-Al-Co [7], et al.

In this investigation, the Sn dendrite firstly solidified from the melt, which lead to the local enrichment of Bi and Pb in the interdendritic region. Meanwhile, the primary Sn-dendrite also provided the nucleation sites for β(Pb_7Bi_3) phase. Therefore, the interdendritic liquid has strong tendency to form β(Pb_7Bi_3)/Sn divorced eutectic firstly. Then, due to the higher degree of supercooling, the β(Pb_7Bi_3)/Sn eutectic forms in the remaining liquid. The quasi-peritectic reaction [L+α-Pb→β(Pb_7Bi_3)+Sn] does not occur as expected due to the non-equilibrium condition.

4 Conclusions

The solidification sequence, constituent phases and directionally solidified microstructure of $Pb_{39}Bi_{25}Sn_{36}$ ternary alloy were characterized. Based on our investigation, the following conclusions can be drawn:

(1) The solidification sequence of $Pb_{39}Bi_{25}Sn_{36}$ alloy begins with the solidification of the primary Sn-dendrite, followed by the divorced eutectic of [$\beta(Pb_7Bi_3)$/Sn]. Then, the monovariant binary [$\beta(Pb_7Bi_3)$/Sn] eutectic is obtained in the interdendritic region. Finally, the remaining liquid undergoes the quasiperitectic reaction [L+$\beta(Pb_7Bi_3)\rightarrow X$+Sn] and ternary eutectic reaction (L$\rightarrow X$+Sn+Bi). The quasi-peritectic reaction [L+α-Pb$\rightarrow\beta(Pb_7Bi_3)$+Sn] does not occur as shown in the ternary phase diagram analysis.

(2) With the increase of withdrawal rate, the as-cast microstructure is significantly refined. As the withdrawal rate increases from 10 to 100 μm·s^{-1}, the primary and secondary dendrite arm spacing (λ_1 and λ_2) reduce from 157.2 and 35.6 μm to 81.8 and 9.0 μm, respectively. Meanwhile, the primary Sn-dendrite is apparently suppressed at the higher withdrawal rate. Particularly, the quenched sample only exhibits the lamellar structure of Sn, $\beta(Pb_7Bi_3)$, and Bi phases.

References

[1] Sha G, O'Reilly K A Q, Cantor B, et al. Quasi-peritectic solidification reactions in 6xxx series wrought Al alloys. Acta Materialia, 2003, 51(7): 1883–1897.

[2] Snugovsky L, Snugovsky P, Perovic D D, et al. Formation of microstructure resulting from quasi-peritectic reactions during freezing of Bi-Pb-Sn and Cu-Ni-Sn ternary alloys. Materials Science and Technology, 2008, 24(2): 245–249.

[3] Ruggiero M A, Rutter J W. Formation of microstructure during solidification of Bi–Pb–Sn ternary eutectic. Materials Science and Technology, 1999, 15(10): 1110–1114.

[4] Perovic D D, Snugovsky L, Snugovsky P, et al. Reactions in Sn corner of Cu-Sn-Zn alloy system. Materials Science and Technology, 2012, 28(1): 120–123.

[5] D'Souza N, Feitosa L M, West G D, et al. Effects of solute trapping on solidification path in Ta-rich Ta-Al-Fe ternary alloys under rapid freezing. Journal of Alloys and Compounds, 2017, 698: 375–383.

[6] D'Souza N, Feitosa L M, West G D, et al. Halo Formation During Solidification of Refractory Metal Aluminide Ternary Systems. Metallurgical and Materials Transactions A, 2018, 49(5): 1749–1761.

[7] Feitosa L M, D'Souza N, West G D, et al. Solidification Reaction Sequence of Co-Rich Nb-Al-Co Alloys. Metallurgical and Materials Transactions A, 2017, 48(8): 3814–3822.

[8] Liu G, Liu L, Zhao X B, et al. Effects of Re and Ru on the Solidification Characteristics of Nickel-Base Single-Crystal Superalloys. Metallurgical and Materials Transactions A, 2011, 42(9): 2733–2741.

[9] Osamura K. The Bi−Pb−Sn (Bismuth-Lead-Tin) system. Bulletin of Alloy Phase Diagrams, 1988, 9(3): 274–281.

[10] Hunt J D. Cellular and primary dendrite spacings. In: Solidification and Casting of Metals Conference, Sheffield, England, 1979: 3–9.

[11] Kattamis T Z, Coughlin J C, Flemings M C. Influence of Coarsening on Dendrite Arm Spacing of Aluminum-Copper Alloys. Transaction of the Metallurgical Society. AIME, 1967, 239: 1504–1511.

[12] Peng P, Li X Z, Li J G, et al. On oscillatory microstructure during cellular growth of directionally solidified Sn-36 at.% Ni peritectic alloy. Scientific Reports, 2016, 6(24315): 1–11.

[13] Liu D M, Li X Z, Su Y Q, et al. Secondary dendrite arm migration caused by temperature gradient zone melting during peritectic solidification. Acta Materialia, 2012, 60(6-7): 2679–2688.

[14] Wang W L, Dai F P, Wei B B. Formation mechanism of primary phases and eutectic structures within undercooled Pb-Sb-Sn ternary alloys. Science in China Series G: Physics, Mechanics and Astronomy, 2007, 50(4): 472–490.

This work was financially supported by the National Natural Science Foundation of China (No. 51604222), China Postdoctoral Science Foundation (No. 152064), Strong Industrial Base Project of China (No. TC160A310-18), Xi'an University of Science and Technology for Excellent Young Teachers Research Program (No. 2018YQ2-12), Excellent Projects funded by Science and Technology Activities for Overseas Students in Shaanxi Province (No. 2018047).